

# Experimental Investigation on the Blast Resistance of Fiber-Reinforced Cementitious Composite Panels Subjected to Contact Explosions

Jeongsoo Nam<sup>1)</sup>, Hongseop Kim<sup>2)</sup>, and Gyuyong Kim<sup>2),\*</sup>

(Received August 18, 2016, Accepted November 6, 2016, Published online February 28, 2017)

**Abstract:** This study investigates the blast resistance of fiber-reinforced cementitious composite (FRCC) panels, with fiber volume fractions of 2%, subjected to contact explosions using an emulsion explosive. A number of FRCC panels with five different fiber mixtures (i.e., micro polyvinyl alcohol fiber, micro polyethylene fiber, macro hooked-end steel fiber, micro polyvinyl alcohol fiber with macro hooked-end steel fiber, and micro polyethylene fiber with macro hooked-end steel fiber) were fabricated and tested. In addition, the blast resistance of plain panels (i.e., non-fiber-reinforced high strength concrete, and non-fiber-reinforced cementitious composites) were examined for comparison with those of the FRCC panels. The resistance of the panels to spall failure improved with the addition of micro synthetic fibers and/or macro hooked-end steel fibers as compared to those of the plain panels. The fracture energy of the FRCC panels was significantly higher than that of the plain panels, which reduced the local damage experienced by the FRCCs. The cracks on the back side of the micro synthetic fiber-reinforced panel due to contact explosions were greatly controlled compared to the macro hooked-end steel fiber-reinforced panel. However, the blast resistance of the macro hooked-end steel fiber-reinforced panel was improved by hybrid with micro synthetic fibers.

**Keywords:** fiber-reinforced cementitious composites, macro hooked-end steel fiber, micro synthetic fiber, contact explosion, blast charge, local damage, fracture energy, panel.

## 1. Introduction

Reinforced concrete (RC) structures, which can be used semi-permanently because of their high strength and high durability, are used for infrastructure and military facilities. RC has comparatively good blast resistant performance compared to other building materials. However, in recent years, terrorist activities and accidental explosions have caused damage to RC structures. These incidents result in the loss of human life and significant damage to properties of national interest (Luccioni et al. 2004; Osteraas 2006; Islam and Yazdani 2008). Blast and impact load caused by explosions and physical conflict must be considered in the design of protective structure systems for improved safety. In the case of local damage of RC panels subject to explosive loads, it is important to suppress the spall of the panel in terms of secondary damage caused by scattering of concrete fragments (McVay 1988). In addition, for high-rise buildings

and plant equipment, local damage caused by explosions or mechanical collisions is likely to lead to continuous collapse, causing additional loss of life and property damage. In this scenario, it is especially necessary to enhance the protection ability of the concrete materials under blast loads.

Research on the anti-blast performance of cement-based composite materials, such as concrete, which has been conducted for application to the protective design of military facilities and infrastructure, has primarily examined the dynamic behaviors of RC under blast loads (Wang et al. 2013; Wu et al. 2009; Silva and Lu 2009). In particular, Morishita et al. (2000), Morishita et al. (2004) and Tanaka and Tuji (2003) reported that the space between reinforcing bars and the compressive strength of concrete were not effective indicators for predicting the local damage and breaking point of a concrete slab through contact-blast testing. Moreover, according to the test results performed by Nam et al. (2011), the blast resistance of RC specimen was obviously not influenced by the reinforcement of steel bar. The local damage of RC specimen was exhibited similarly to the results of the non-fiber-reinforced high strength concrete specimen. These results indicate that other methods should be considered to reduce the damage of concrete panels by blast loads.

For decades, previous studies have utilized fiber-reinforced composites at both material and structural levels to improve the blast and impact resistance of cement-based composite materials (Yamaguchi et al. 2011; Silva and Lu 2007; Ohkubo et al. 2008; Ha et al. 2011; Wu et al. 2009;

<sup>1)</sup>Laboratory for Materials and Structures, Tokyo Institute of Technology, Yokohama 226-8503, Japan.

<sup>2)</sup>Department of Architectural Engineering, Chungnam National University, Daejeon 34134, Korea.

\*Corresponding Author; E-mail: gyuyongkim@cnu.ac.kr

Mosalam and Mosallam 2001; Razaqpur et al. 2007; Xie et al. 2014; Ohtsu et al. 2007; Lan et al. 2005; Soe et al. 2013; Nam et al. 2010; Kim et al. 2015; Li et al. 2016; Coughlin et al. 2010; Yoo et al. 2015; Kim et al. 2015; Yoo and Yoon 2016; Nam et al. 2016). Yamaguchi et al. (2011) reported that polyethylene fiber-reinforced concrete has superior blast resistance under contact explosions as compared with normal RC. Silva and Lu (2007) examined the blast resistance of RC slabs containing fiber-reinforced polymers (FRP). The fiber reinforcing was applied on one or both sides and subjected to a close-in blast test. The explosion resistance of RC slabs was improved by the inclusion of FRP, and the effect of reinforcement on both sides was found to have a larger effect than reinforcement of only one side. Ohkubo et al. (2008) used contact-blast testing to identify the reduction of spall due to applying a reinforcing carbon fiber sheet and an aramid fiber sheet on the back side of a concrete slab. Ha et al. (2011) also used a close-in blast test to evaluate the reduction of fracture of concrete panels due to reinforcement with CFRP and polyurea (PU). To control the destruction and suppressed cracking, it is necessary to review the blast resistance of the fiber-reinforced cementitious composites (FRCCs). Wu et al. (2009) evaluated the explosion resistance of slabs manufactured with both ultra-high performance fiber concrete (UHPC) and reinforced ultra-high performance fiber concrete (RUHPC). The blast resistance of the RUHPC slab was good compared to the other concrete slabs in the close-in blast tests. However, there have been very limited studies on the local damage of FRCC panels with various blended fibers and comparison of their blast resistance to that of conventional concrete.

For blast tests of cementitious composite materials, the failure modes are influenced by the standoff distance from the explosion source. The effect of blast load on the test specimens decreases with atmospheric pressure and the dispersion of explosion pressure increases with the distance from the explosion source. Furthermore, the mass of high explosive (HE) is also serves as a very important parameter in the failure modes of cementitious composite materials. Therefore, the scaled distance with the mass of HE has a significant impact on the failure modes of cementitious composite materials under the explosion test. In the close-in blast test, generally induces global damage of the test specimen, such as flexural failure, cracking, and shear-punching action, based on the standoff distance level. However, local damage (i.e., crater, spall, and breach) also will occur if the combined loads are severe enough (McVay 1988), although that require larger blast charge compared to the contact blast test. In contrast, the failure modes of cementitious composite materials caused by contact-blast tests tend to be local damage. Thus, the current study employs contact explosions because various strengths of blast charge are required; namely, when considering the explosion tests on a laboratory scale, the local damage of the concrete panel caused by the close-in blast test is difficult to perform, whereas the evaluation of local damage is possible with only a small amount of blast charge in contact explosions.

In particular, the spall damage on the back side of a structure is closely related to the fracture energy; thus, the damage of FRCCs under contact explosions must be evaluated to consider the blast resistance according to the development of fracture energy. Additionally, since the strain rates of cementitious composite materials under contact explosions are approximately  $1000\text{--}0,000\text{ s}^{-1}$ , it is very difficult to evaluate the dynamic properties of cementitious composite materials under contact explosions. Thus, the static fracture energies of cementitious composite materials are considered in order to examine the dynamic fracture energy. The dynamic fracture energy is approximately the same as the static fracture energy (van Doormaal et al. 1994; Lee and Lopez 2014).

Due to FRCC indicates superior energy absorption capacity, very low crack widths, and high ductility, it can be expected a suitable safety performance as protective structures more than conventional concrete under extreme loadings such as high-velocity impacts and explosions. However, very few investigations of the blast resistance of FRCC panels under contact explosions have been conducted. Accordingly, in this study, the local damage of FRCC panels with blended fibers was investigated after exposure to contact explosions, and the relationship between the static fracture energy and failure mode was examined. To clarify the blast resistances of FRCC panels, plain panels, such as non-fiber-reinforced high strength concrete (NHC), and non-fiber-reinforced cementitious composites (NCC) were also tested. In addition, the hybrid effect of micro synthetic fibers and macro hooked-end steel fibers in FRCCs was investigated. Moreover, the experimental results were examined through comparison with existing damage evaluation prediction equations for prediction of the limited thickness on the local damage of panels subjected to contact explosions.

## 2. Experimental Program

The experiments were designed to evaluate the blast resistance of FRCC panels compared with plain panels. The used materials, the test specimen preparations, and the applied test procedures for the experimental measurements are discussed in this section.

### 2.1 Materials and Mixture Proportions

The employed materials are summarized in Table 1. Type II Ordinary Portland cement (ASTM 2016) was used as the binder for the cementitious materials. In the case of NCC and FRCCs, class-F fly ash (ASTM 2015) was used as 15% of the total binder to improve the workability (Yang et al. 2007; Mahmoud et al. 2013). The mixture proportions for NHC and NCC are shown in Table 2. The water/binder ratio (W/B) of NHC was 0.3, and that of NCC was 0.4. The unit weight of the binder used for NHC was  $533\text{ kg/m}^3$ , and that used for NCC was  $1129\text{ kg/m}^3$ . A polycarboxylic acid-based high-range water reducer (HRWR) was used to achieve the target flow for each fresh cementitious composites.

**Table 1** Material properties.

Materials	Properties
Cement	Ordinary Portland cement (Type II), density: 3.15 g/cm <sup>3</sup> , fineness: 3770 cm <sup>2</sup> /g
Fly-ash (used for NCC and FRCCs)	Class-F type, density: 2.30 g/cm <sup>3</sup> , fineness: 3228 cm <sup>2</sup> /g
River sand (used for NHC)	Density: 2.54 g/cm <sup>3</sup> , absorption ratio: 1.01%
Silica sand (used for NCC and FRCCs)	Density: 2.64 g/cm <sup>3</sup> , absorption ratio: 0.38%, class-7
Crushed coarse aggregate (used for NHC)	Maximum size: 20 mm, density: 2.65 g/cm <sup>3</sup> , absorption ratio: 1.39%

**Table 2** Mixture proportions of plain specimen.

ID	W/B	Cement (kg/m <sup>3</sup> )	Fly-ash (kg/m <sup>3</sup> )	Water (kg/m <sup>3</sup> )	Coarse aggregate (kg/m <sup>3</sup> )	River sand (kg/m <sup>3</sup> )	Silica sand (kg/m <sup>3</sup> )	HRWR (kg/m <sup>3</sup> ) <sup>a</sup>
NHC	0.3	533	–	160	948	750	–	4.3
NCC	0.4	960	169	452	–	–	395	0.0

NHC non-fiber-reinforced high strength concrete, NCC non-fiber-reinforced cementitious composite.

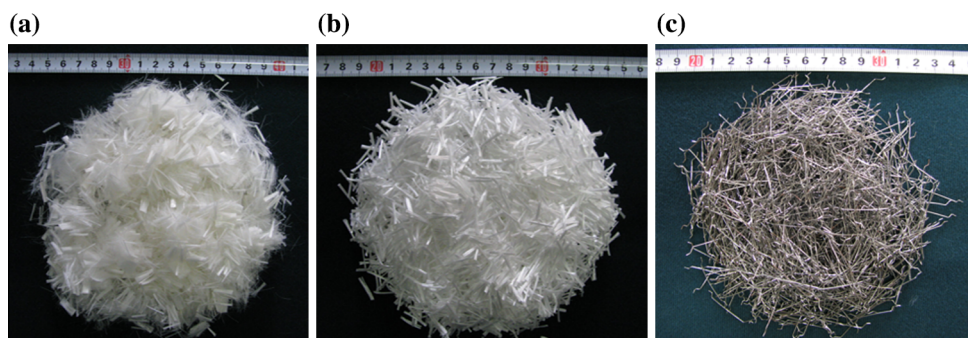
<sup>a</sup> High-range water reducer, target value of flow in NHC: 550 ± 50 mm, target value of flow in NCC: 170 ± 20 mm.

Except for the blended fibers, the mixed materials of the FRCCs were the same as those of the NCC, as described in Table 1. Table 3 shows the properties of the fibers used in this study. Pictures of the used fibers are shown in Fig. 1. Two kinds of micro synthetic fibers, i.e., polyvinyl alcohol (PVA) fiber and polyethylene (PE) fiber, were used in the preparation of the PVA fiber-reinforced cementitious composite (PVACC) and the PE fiber-reinforced cementitious composite (PECC), respectively. Additionally, macro hooked-end steel fibers of 30 mm in length and 0.7 mm in diameter were used for the steel fiber-reinforced cementitious composite (SCC) panels. Table 4 shows the mixture proportion of the FRCCs. The

fibers were blended at 2% of the total volume, and other properties, such as W/B and binder, were applied to the panels under the same conditions as the NCC panels. Moreover, hybrid FRCC panels were manufactured with the micro synthetic fibers and macro hooked-end steel fibers. The hybrid FRCC panels are denoted with PVASCC (indicating a hybrid of micro PVA fibers and macro hooked-end steel fibers) and PESCC (indicating a hybrid of micro PE fibers and macro hooked-end steel fibers) followed by the hybrid fibers type, and the proportions of the hybrid materials were composed in a 1:1 ratio. This series was considered for the hybrid effects of micro and macro fibers under contact explosions.

**Table 3** Properties of fibers.

Fiber type	Specific density (g/cm <sup>3</sup> )	Length (mm)	Diameter (mm)	Tensile strength (MPa)
PVA	1.30	12	0.040	1300
PE	0.95	15	0.012	2700
Steel	7.85	30	0.700	1140

**Fig. 1** Pictures of fibers; a polyvinyl alcohol (PVA), b polyethylene (PE), c hooked-end steel.

**Table 4** Mixture proportions of FRCC specimen.

ID	W/B	Cement (kg/m <sup>3</sup> )	Fly-ash (kg/m <sup>3</sup> )	Water (kg/m <sup>3</sup> )	Silica sand (kg/m <sup>3</sup> )	Fibers (V <sub>f</sub> , %)	HRWR (kg/m <sup>3</sup> ) <sup>c</sup>
PVACC	0.4	960	169	452	395	2	16.9
PECC	0.4	960	169	452	395	2	22.6
SCC	0.4	960	169	452	395	2	5.6
PVASCC	0.4	960	169	452	395	2 (1) <sup>a</sup>	11.3
PESCC	0.4	960	169	452	395	2 (1) <sup>b</sup>	16.9

*PVACC* PVA fiber-reinforced cementitious composite, *PECC* PE fiber-reinforced cementitious composite, *SCC* Steel fiber-reinforced cementitious composite, *PVASCC* Hybrid fiber-reinforced cementitious composite (PVA fibers + Steel fibers), *PESCC* Hybrid fiber-reinforced cementitious composite (PE fibers + Steel fibers).

<sup>a</sup> The total volume (share of PVA fiber).

<sup>b</sup> The total volume (share of PE fiber).

<sup>c</sup> High-range water reducer, target value of flow in FRCCs: 170 ± 20 (mm).

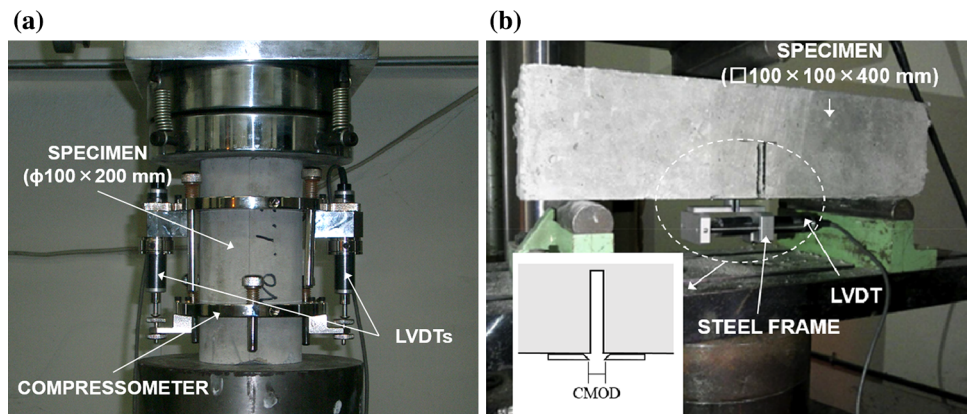


**Fig. 2** Test setup of static mechanical properties; **a** compression test by cylindrical specimen, **b** static fracture energy test by notched specimen.

## 2.2 Test Setup and Procedure

### 2.2.1 Static Mechanical Tests

Figure 2 shows the experimental set up for compression and static fracture energy testing of the cementitious composite specimens. The compressive strength and the elastic modulus were evaluated in accordance with ASTM C 39 (ASTM 2015) and ASTM C469 (ASTM 2014), and determined from standard cylindrical specimens of 100 mm in diameter and 200 mm in height. The compression tests were performed using a universal testing machine (UTM) and a compressometer with linear voltage differential transformers (LVDTs). The flexural properties of each notched specimen were performed according to RILEM 50-FMC Draft Recommendation (RILEM 50-FMC Draft Recommendation 1985) to determine the fracture energy of the fiber-reinforced concrete. Each specimen had a notch at the center of the prismatic specimen, which were cut by using a circular diamond concrete saw. The fracture energy (energy absorption capacity) was determined using Eq. (1):

$$G_F = (W_0 + mg\delta_0)/A_{lig}. \quad (1)$$

where  $G_F$  is the fracture energy (Nm/m<sup>2</sup>),  $W_0$  is determined from the crack-mouth opening displacement (CMOD) based on the area of the load (Nm),  $m$  is  $m_1 + 2m_2$ ,  $m_1$  is the mass

of the specimen between the supports (kg),  $m_2$  is the mass of the part of the loading arrangement that is not attached to the machine,  $g$  is acceleration due to gravity (9.81 m/s<sup>2</sup>),  $\delta_0$  is the final deformation of the specimen (m), and  $A_{lig}$  is the cross-sectional area of the fracture (m<sup>2</sup>).

The mechanical properties were evaluated after ageing for 28 days following curing in an environmental chamber at a temperature of 23 ± 2 °C and a relative humidity of 60 ± 5%.

### 2.2.2 Contact-Blast Tests

The damage of plain panels under contact explosions was evaluated for failure modes such as crater, spall, and breach. The failure modes of the plain panels were obtained according to amount of blast charge for the contact blast tests using emulsion explosives. Observations of how the amount of blast charge affected the failure mode of plain panels were made, and a suitable amount of blast charge for damage evaluation was determined. From evaluating the damage results of plain panels, the amount of blast charge for contact blast tests of FRCC panels was determined. In this study, emulsion explosives (NewMITE Plus) were used in contact blast tests because they are chemically very safe and easy to cast (Hanhwa Corporation/Explosive 2016). For emulsion explosives, the thermal energy is 4.61 MJ/kg, which is

calculated by heat of explosion (1100 kcal/kg) of NewMITE Plus. In addition, the value of the thermal energy of TNT was used 4.29 MJ/kg with reference to the previous work by Morishita et al. (2000, 2004). Thus, the ratio of the thermal energy between TNT and emulsion explosives is 1.07. In later discussions, the mass of the emulsion explosive is converted to equivalent TNT mass by means of this ratio.

As shown in Fig. 3, the dimensions of the plain and FRCC panels were 1000 mm × 1000 mm × 100 mm. To conduct the contact blast tests, emulsion explosives with a semi-elliptical shape were placed in the centers of the upper surfaces of the panels and connected with an electric detonator. Based on the pre-investigations for the influences by installation direction of the electric detonator, the range the mass of the blast charges used in the contact explosions, the influences of the detonator is regarded not prominent and can be neglected. Emulsion explosives of 50, 75, 100, 200, 400, and 800 g were used for the contact blast tests of the NHC, and emulsion explosives of 50 and 100 g were used for the NCC. The contact explosions of the FRCC panels were performed with blast charges of 100 and 200 g. The design of the blast charges for the FRCC panels was based on the failure modes of the plain panels, which will be discussed in Sect. 3.2.

Figure 4 shows the method for evaluating the local damage, such as crater, spall, and breach, in the front and back sides of a panel. The diameter and depth of the local damage were calculated from the mean values for the crater and spall measurements. The extent of the surface damage to each panel was quantified graphically by mapping the local damage on the front and back sides and comparing the damage area, A2, to the total area, A1 + A2.

### 3. Experimental Results and Discussion

#### 3.1 Static Mechanical Properties

The test results were presented as the mean of the values obtained for each of the three specimens. The static

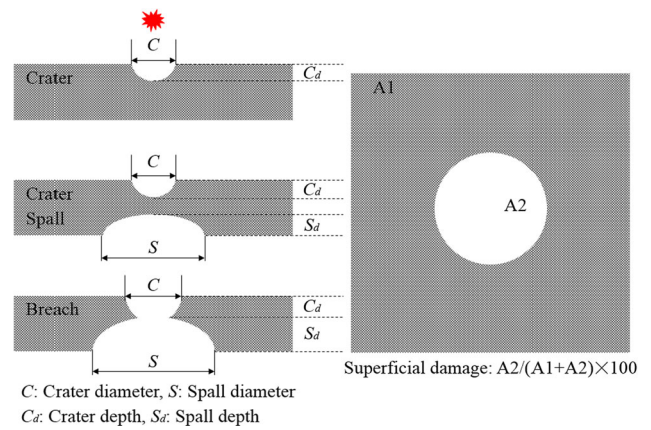


Fig. 4 Measurement of damage areas in the panels.

mechanical properties of cementitious materials are shown in Table 5. The compressive strength of NHC was 64.3 MPa and that of NCC was 43.7 MPa. The compressive strength in all of the FRCCs was less than that of the NCC, and the range of compressive strengths was 27.9–36.7 MPa. The compressive strengths of PVASCC and PESCC were evaluated at 35.8–36.7 MPa, respectively; moreover, the steel fibers in the hybrid samples provided a strength-enhancing effect as compared to the specimens that only used PVA fiber or PE fiber. The elastic modulus of the FRCCs were less than those of plain specimens, following almost similar proportions as the compressive strength. Generally, the blended fibers did not improve the elastic modulus of the FRCCs because the cementitious matrix was made without coarse aggregate (Atiş and Karahan 2009; Naaman 2003). In addition, these results can be explained by the interfacial transition zone (ITZ) between the cementitious matrix and the blended fiber, as the ITZ was made in a relatively weak layer and large pores due to the blended fibers exist in the cementitious composites matrix (Li and Stang 1997). Meanwhile, the fracture energy of all of the FRCCs increased as compared to NHC and NCC. For FRCCs, the fracture energy, which was calculated by the area below the

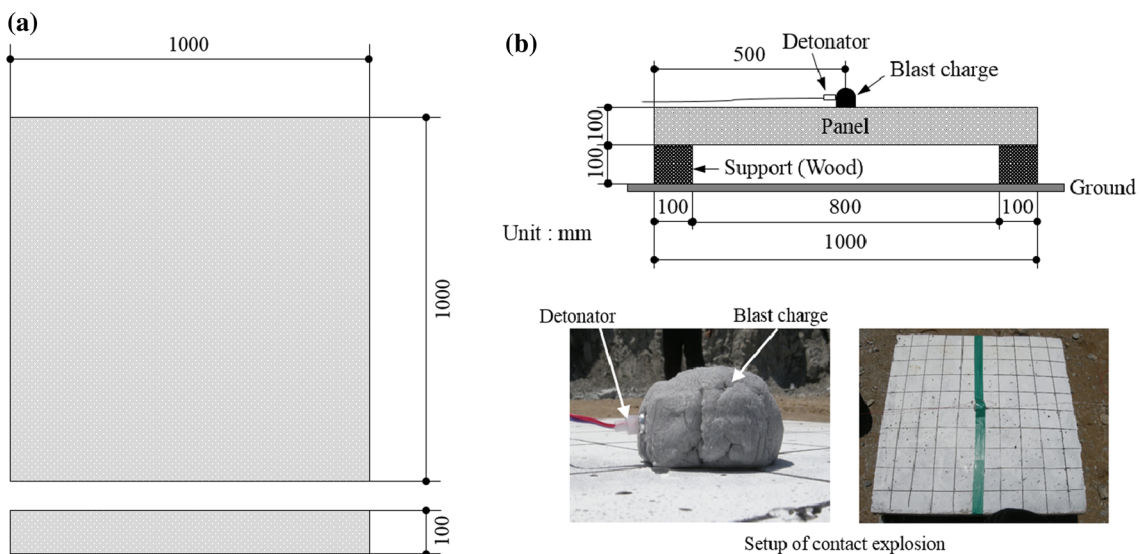


Fig. 3 Experimental setup of blast resistance; a dimension of panel, b contact explosion.

**Table 5** Test results of static mechanical properties (standard deviation).

ID	Compressive strength (MPa) <sup>a</sup>	Elastic modulus (GPa) <sup>a</sup>	Fracture energy (N·m/m <sup>2</sup> ) <sup>a</sup>
NHC	64.3 (3.6)	38.5 (2.1)	804 (160.3)
NCC	43.7 (2.8)	23.3 (1.4)	753 (118.6)
PVACC	28.5 (1.5)	15.5 (0.8)	18,898 (578.5)
PECC	27.9 (1.7)	13.2 (0.7)	38,996 (1805.4)
SCC	34.7 (2.2)	19.1 (0.8)	13,002 (342.2)
PVASCC	35.8 (1.8)	18.6 (0.6)	18,592 (466.7)
PESCC	36.7 (1.6)	14.1 (0.6)	25,479 (1251.3)

<sup>a</sup> An average value of three time tests at 28 days.

load—CMOD curve, was higher in PVACC and PECC compared to SCC. This is ascribed to the higher post-crack stress and residual stress of PVACC and PECC, given that fracture energy greatly depends on the stress-sustaining capacity along with the maximum flexural stress. In addition, the fracture energy of hybrid FRCCs decreased as compared with PVACC and PECC. When compared with PVACC or PECC, the reduction of the fracture energy by hybrid of blended fibers in PESCC is greater than that of PVASCC. These results can be explained by the difference of the fracture energy between PECC and SCC. Similar observations were previously reported by Ahmed et al. (2007). In the case of a hybrid fiber-reinforced cementitious composite, the reduction of the flexural capacity is dependent on the hybrid ratio between high performance and low performance under identical volume ratio of fiber reinforcement. PECC has fracture energy about 3 times greater than that of SCC, whereas PVACC has fracture energy about 1.5 times greater than that of SCC. Thus, it can be said that the reduction of the fracture energy in PESCC was clearly observed compared to that of PVASCC. Nevertheless, PESCC has fracture energy about 2 times greater than that of SCC, which shows the significant influence of hybrid macro and micro fiber on FRCC flexural performance.

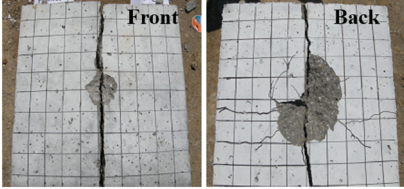
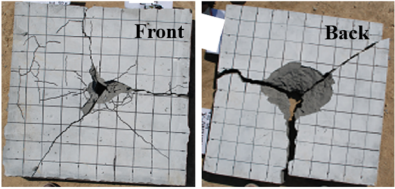
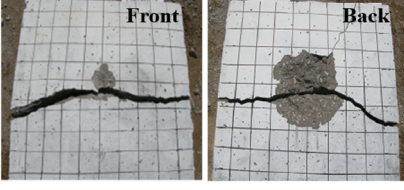
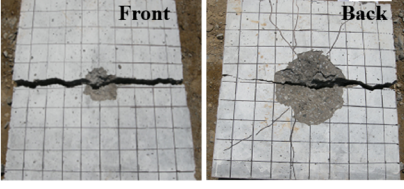
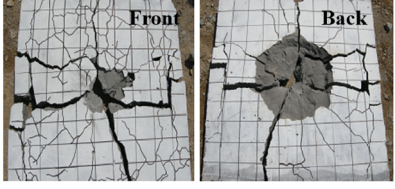
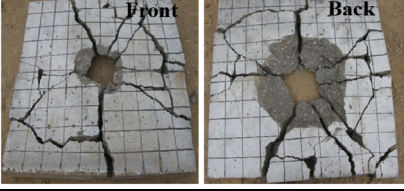


### 3.2 Blast Resistance

#### 3.2.1 Appearance of the Damage

The results of the contact blast tests of NHC and NCC are shown in Fig. 5. For the NHC panels, spall failure was observed for blast charges of 50, 75, and 100 g. Similar observations were previously reported by Ohkubo et al. (2008): in the case of TNT blast charges of 50 g, significant large spall was apparent in the concrete panel. As seen in Fig. 5, breach failure of the NHC panel occurred in the case of contact explosion with a blast charge of 200 g. Therefore, the primary failure mode of the local damage in the NHC panels transitions between 100 and 200 g of blast charge. In addition, for blast charges of 400 and 800 g, the quantitative failure modes of crater, spall, and breach were not observed in NHC panels under contact explosions. This also means that it is inappropriate to compare failure modes with the local damage of FRCC panels at these blast charge masses. Furthermore, the failure modes of NCC panels were also

investigated. The NCC panels had the same mixture proportions as compared with FRCC panels except for the blended fibers. For NCC panels, breach failure was observed at both 50 and 100 g of blast charge. The local damage in the NCC panels increased according to the amount of blast charge. Therefore, these results on the local damage of NCC panels are useful for comparison with the failure mode of FRCC panels. When the failure mode of NCC panels was compared with NHC panels at both 50 and 100 g of blast charge, NCC panels, breach failure was observed with severe cracks. Whereas the failure mode of breach was not generated in NHC panels. These results can be explained by the difference of the compression behaviors and used materials. NHC has an approximately 1.5 times greater compressive strength and elastic modulus than those of NCC. In addition, NCC panel does not contain coarse aggregate of high rigidity. It is believed that the difference of the compression behaviors and used materials between NHC and NCC in contact explosions without fiber reinforcement which in turn may influence the failure modes at the identical blast charges. Based on the above discussion regarding the local damage in the NHC and NCC panels, the amount of blast charge for damage evaluation of FRCC panels subjected to contact explosions should be less than 400 g of emulsion explosive; thus, FRCC panels were investigated with blast charges of 100 and 200 g.

The external damage of FRCC panels with blended fibers is shown for each blast charge in Fig. 6. The results of the NHC panels were plotted for comparison with the failure modes of FRCC panels. Hence, the blast resistance of the FRCC panels under contact explosions can be clarified from the figure. For each FRCC panels that used a blast charge of 100 g, spall failure was not observed in the overall panels. It is evident from the figure that the blast resistance of the FRCC panels was significantly improved compared to the NHC panels. Additionally, among the FRCC panels, the SCC panels exhibited crack patterns on their back sides that were more significant than the other FRCC panels, indicating that the static flexural behavior, such as strain-hardening performance, of SCC contributed to the crack pattern under dynamic blast loading. Generally, macro hooked-end steel fiber reinforced composites have low strain-hardening capacity as compared to micro synthetic fiber reinforced

Specimen ID	NHC	NCC
50 g		
75 g		-
100 g		
200 g		-
400 g		-
800 g		-

**Fig. 5** Appearance of the damage in NHC and NCC panels for each blast charge.

cementitious composites. However, amount of cracks in the SCC panel was reduced by hybrid with micro synthetic fibers. This improvement was provided from a one-to-one hybrid ratio of macro hooked-end steel fibers and micro synthetic fibers. In addition, all FRCC panels experienced spall failure mode in the case of contact explosions using 200 g blast charges, but the degree of spall was very slight compared to the plain panels.

The failure modes of all panels are summarized for each blast charge in Fig. 7. As the damage of the investigated panels increased with the amount of explosives, spall and breach become the critical failure modes. However, from the figure, the failure modes of the FRCC panels were one stage less severe compared to the NHC and NCC panels. This demonstrates that FRCCs have superior blast performance compared to NHC and NCC under contact explosions of the

same blast charge. Therefore, FRCCs should provide more blast resistance when used as a protective material.

### 3.2.2 Diameter, Depth, and Superficial Damage

To clarify the effect of fiber reinforcement on the blast resistance of FRCC panels, quantitative damage results were provided through measurements of diameter, depth, and superficial damage. The measured diameters of crater and spall are shown for each blast charge in Fig. 8. It is clear from the figure that the damage diameters of the FRCC panels were significantly smaller than the plain panels after contact explosions using blast charges of 100 g. In addition, in the case of a 200 g blast charge, the diameter of spall in all FRCC panels was less than 300 mm, which is approximately half of that of the NHC panel. Compared with the PVACC and PECC panels, the hybrid FRCC panels exhibited larger

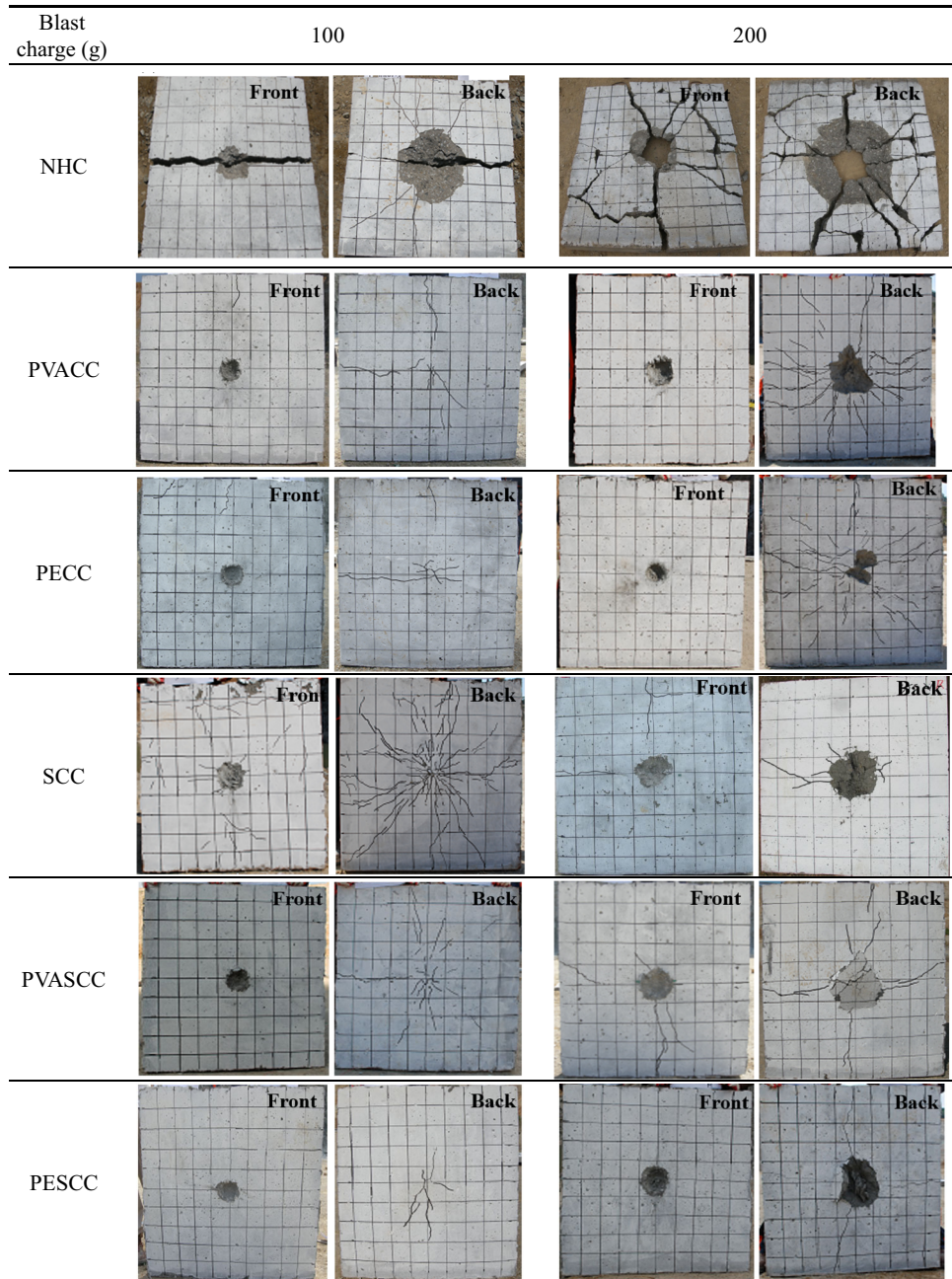


**Fig. 6** Appearance of the damage in NHC and FRCCs panels for each blast charge.

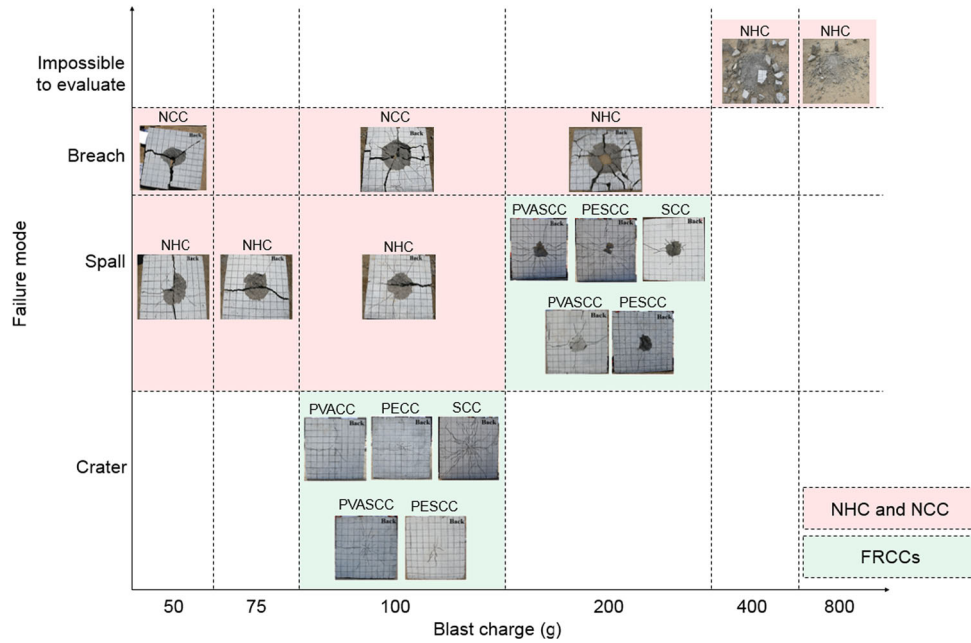
spall diameters. The hybrid FRCC panels can have a relatively small specific surface area between the fibers and cementitious matrix as compared to the PVACC and PECC panels in the same conditions. The number of blended fibers in the hybrid FRCC is approximately half that of the PVACC and PECC panels. Previous research (Yamaguchi et al. 2011), on fiber-reinforced concrete specimens subjected to contact blast tests showed that as fiber volume fractions increase, the damage diameters of the back sides decreased. This implies that the specific surface area between the blended fibers and the cementitious matrix is strongly correlated with the diameter of local damage.

The depth of the crater and spall due to the contact explosions of the 100 and 200 g blast charges are shown in Fig. 9. For FRCC panels under contact explosions using 100 g blast charges, the crater depth was less than that of the

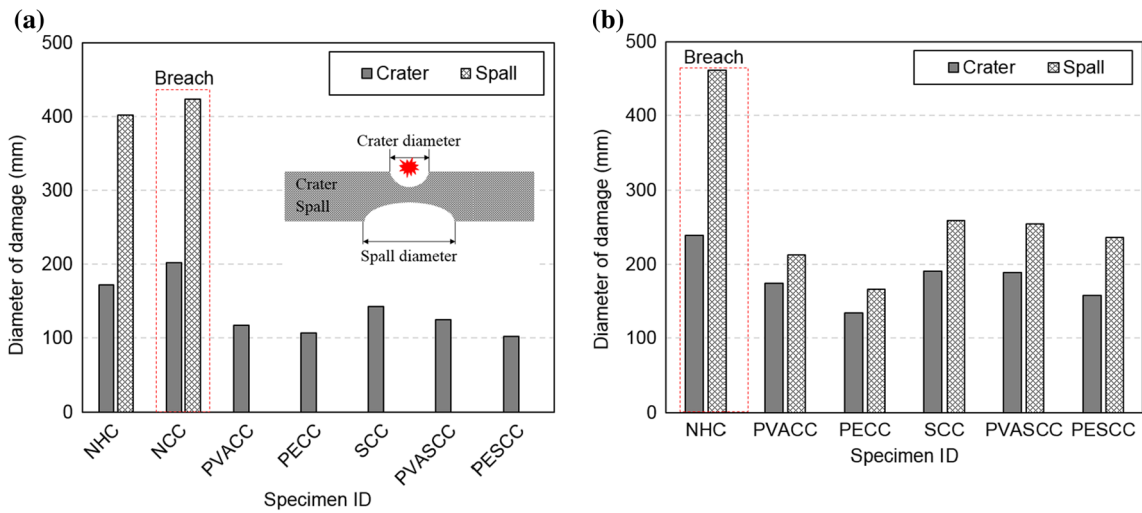
NCC panel, and that of the spall was immeasurable. Figure 10b describes the depths of the crater and spall for each panel after contact explosions using 200 g blast charges. From this figure, the fiber reinforcements make the depths of the crater and spall slightly smaller than those of the NHC panel. The resistance effect of FRCC panels on the depths of crater and spall was not clearly observed compared to resistance observed for the diameters in the 200 g blast charge (see Fig. 8). The resistance for crater depth in the panels was likely influenced both by the fiber reinforcements and by the compressive strengths of the test materials. Even though the compressive strengths of the FRCC panels were less than those of the plain panels, the crater depths of the FRCC panels were also less than those of the plain panels.

Figure 10 shows the ratio of the crater depth to panel thickness ( $C_d/T$ ) for the failure modes of the plain and FRCC





**Fig. 7** Failure mode of all panels for each blast charge.



**Fig. 8** Diameter of damaged areas for each blast charge; **a** 100 g, **b** 200 g.

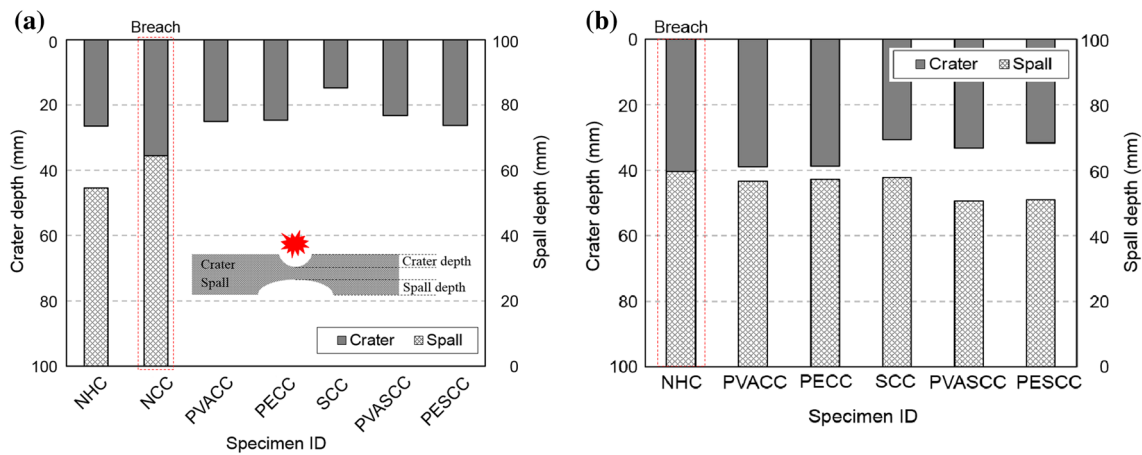


**Fig. 9** Depth of damaged areas for each blast charge; **a** 100 g, **b** 200 g.

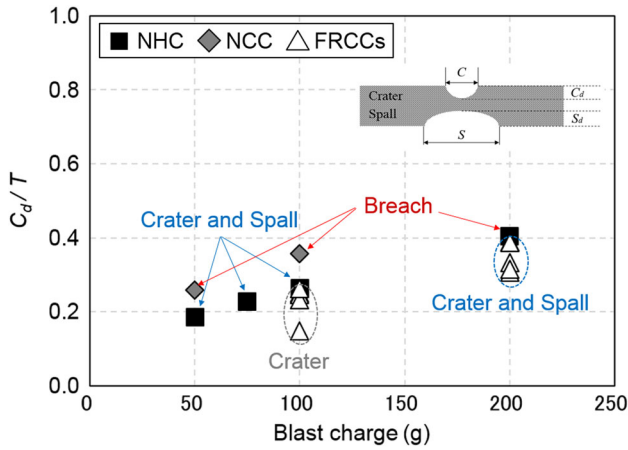


**Fig. 10** Failure mode of panels by relationship between  $C_d/T$  and each blast charge.

panels. The NCC panel experienced breach failure with a  $C_d/T$  of 0.26 at 50 g of blast charge. For the NHC panels, the spall failure had a  $C_d/T$  less than 0.4, whereas the breach failure had a  $C_d/T$  greater than 0.4. In contrast, for the FRCC panels, crater failure occurred in the range of  $C_d/T$  values for which spall failure was observed in the NHC panel, and spall failure occurred in the range of  $C_d/T$  values for which breach failure was observed in the NCC panel. Therefore, the blended fibers in the FRCC panels play an important role for blast resistance under contact explosions.

Figure 11 shows the superficial damage on the front and back sides of the panels for each blast charge. The superficial damage on the back side of the FRCC panels, when using the 100 g blast charge, was calculated from the lengths and widths of the cracks. Among the FRCC panels, the SCC panel exhibited the most superficial damage under contact explosions using 100 g of blast charge. However, the amount of superficial damage in the SCC panel was only approximately 1%, which occurred on both the front and back sides. Moreover, this value is very small compared to superficial damage to the NCC panel. Furthermore, in the cases of contact explosions using 200 g blast charge, the FRCC panels experienced significantly less superficial

damage compared to the NHC panel. For the FRCC panels, the superficial damage on the back side was less than 5%, whereas that of NHC panel was approximately 18%. Based on the obtained results, the superficial damage was proportionally related to the damage diameter. Therefore, the fiber reinforcement in the FRCCs also helps restrain the surface progress of local damage.

Figure 12 shows the relationship between the fracture energy and the superficial damage on the back side of the panels for each blast charge. It is clear from the figure that the growth of the fracture energy of the FRCCs contributed to constraining the superficial damage. In both cases, the reduction of superficial damage is highly correlated with fracture energy. In addition, in the case of a 100 g blast charge, the superficial damage of the SCC panel was improved by hybrid with PVA or PE fibers, as the fracture energy of the PVASCC and PESCC was significantly higher than that of the SCC. The increase of the fracture energy in the FRCCs contributed to the development of their flexural capacity, which greatly reduced the local damage caused by the contact explosion to the back side of the panel. It can be said that the mechanism of spall failure in cementitious composites is different from the static mechanical characteristics, however, the improvement of the static fracture energy can have an indirect effect to enhance the blast resistance under contact explosions. Previous studies on the effectiveness of fracture energy for improving the spall resistance of cementitious composite materials subjected to contact explosions are very limited. However, in some studies on the impact resistance of cementitious composites under dynamic loading, the effects of fracture energy on scabbing resistance are observed (Leppänen 2006; Mechtcherine et al. 2011; Zhang et al. 2009; Habel and Gauvreau 2008; Mindess et al. 1987). Improving the fracture energy of cementitious composites has a large effect on the reduction of scabbing failure, which especially has a significant influence on the reduction of the diameter compared to the depth of local damage. Additionally, because the fracture energy depends on the loading rate, the dynamic fracture energy in blast loading, such as contact explosions,

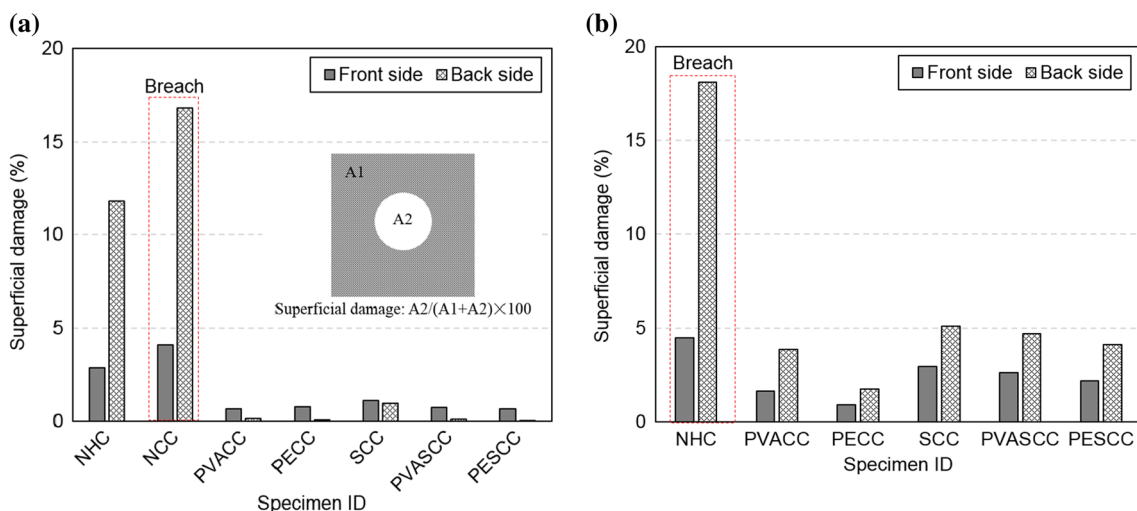


**Fig. 11** Superficial damage of panels for each blast charge; a 100 g, b 200 g.

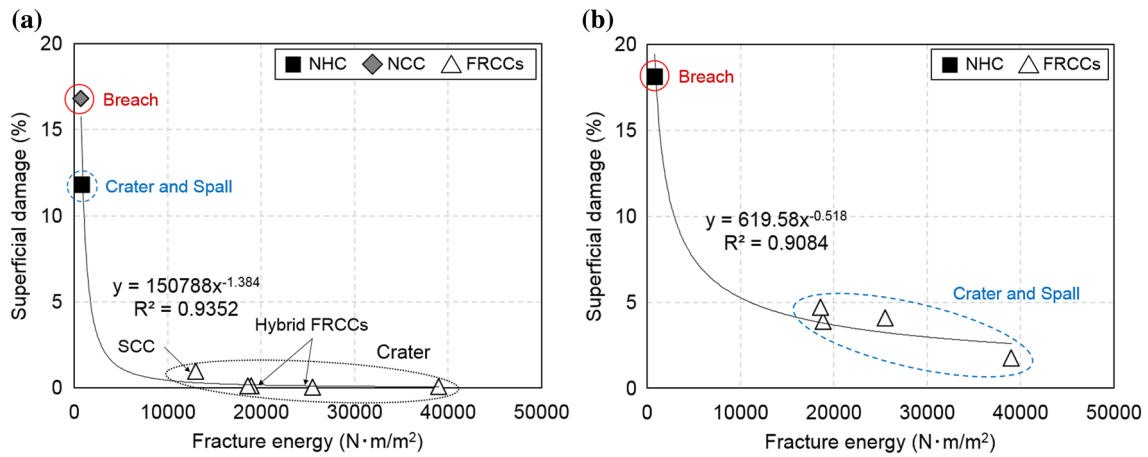


**Fig. 12** Relationship between the fracture energy and the superficial damage on the back side of the panels for each blast charge; a 100 g, b 200 g.



**Fig. 13** Fragment of the back side of the PVASCC panel in case of blast charge of 200 g.

can affect the local damage characteristics of cementitious composites compared to those of static loading conditions.

A fragment of the back side of the PVASCC remained attached to the panel, as shown in Fig. 13. From the figure, the spall fragment bulged approximately 45 mm from the panel and did not detach completely. Likewise, the blast resistance of the hybrid FRCC panels under contact blast tests using 200 g of blast charge exhibited equivalent performance as compared with those of the PVACC and PECC panels. Based on the obtained results, it is obvious that the hybrid effect of the blended fibers and their characteristics plays an important role in the blast resistance of PVASCC and PESCC panels. The hybrid effect of the macro and micro fibers in the FRCCs is discussed in several previous studies: the hybrid blend of macro and micro fibers improved the mechanical properties of FRCCs (Shu et al. 2015; Lawler et al. 2003). The cementitious composite materials reinforced with a hybrid blend of macro and micro fibers showed better mechanical performance than those that were only reinforced with macro fibers. Consequentially, these aspects explain the improvement of the blast resistant performance of hybrid FRCC panels. For the FRCC panels, the reduction of spall is dependent on the control of macro cracking under blast load. Figure 14 shows a schematic of the hybrid blend effects of macro and micro fibers on the blast resistance of FRCCs. In the hybrid FRCC panels, the micro fibers were most effective at limiting the widening of

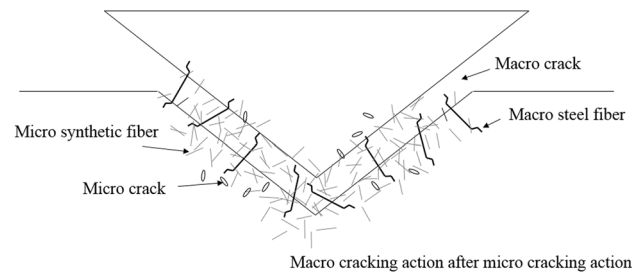


**Fig. 14** Influence of hybrid fiber reinforcement on the spall damage.

cracks. Furthermore, the micro fibers assisted the strain capacity of the macro fibers in the FRCC panels. In addition, the improvement of flexural performance significantly influenced the local damage reduction of the FRCCs. From the results previously described in Sect. 3.1 on the comparative evaluation of the flexural properties between FRCCs and plain specimens, the fracture energy of FRCCs significantly increased as compared to NHC and NCC.

### 3.2.3 Relationship Between Diameter and Depth of Local Damage

To clarify the resistance of FRCC panels to critical local damage, such as spall, the diameter and depth of local damage are compared in Fig. 15. It is clear from the figure that the diameter/depth ratio of local damage for the

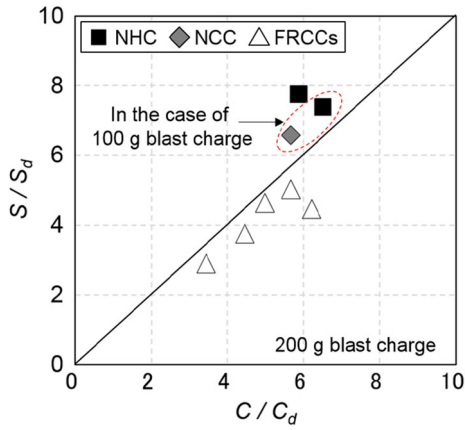


**Fig. 15** Relationship between crater and spall calculated from diameter/depth ratio.

plain panels was more closely distributed in spall areas under contact blast tests in the cases of both 100 and 200 g of explosives, which means that the spall of the back side contributed most of the damage. Conversely, the diameter/depth ratio of local damage for the FRCC panels was more closely distributed in crater areas. It is obvious from the figure that the diameter/depth ratio of the local damage increased proportionally, but the amount of spall area is not critical in contrast to that of the plain panels. Based on the above discussion, FRCCs should experience a reduced damage area on the back side of panels even if spall or breach occurs.

### 3.2.4 Comparison of Experimental Results with Empirical Equations for Failure Mode

Morishita et al. (2000, 2004) proposed useful equations for estimating the failure mode in normal RC slabs subjected to contact explosions. In the following discussions, the experimental results of local damage are compared to the equations of Morishita et al.

The scale thickness of a concrete panel ( $T/W_m^{1/3}$ ) using emulsion explosives can be obtained as given in the following equation:

$$\frac{T}{W_m^{1/3}} = \frac{T}{W^{1/3}} \cdot \left( \frac{K_{\text{TNT}}}{K} \right)^{1/3} \quad (\text{unit: cm/g}^{1/3}) \quad (2)$$

where  $T$  is thickness of concrete,  $W_m$  is the substitution amount of explosive,  $K_{\text{TNT}}$  is Chapman–Jouguet (C–J) thermal energy ( $\approx 4.29$  MJ/kg) of TNT, and  $K$  is the C–J thermal energy (MJ/kg) of the used explosive. The C–J thermal energy of emulsion explosives is 4.61 MJ/kg.

The range of the local damage is limited, depending on  $T/W_m^{1/3}$ , for crater, spall, and breach. It can be calculated from the following equations:

$$\frac{C_d}{T} = -0.046 \frac{T}{W_m^{1/3}} + 0.42 \quad (3)$$

$$\frac{C_d + S_d}{T} = \frac{C_d}{T} \quad \left( \text{only crater } 3.6 \leq \frac{T}{W_m^{1/3}} \right) \quad (4)$$

$$\frac{C_d + S_d}{T} = -0.49 \frac{T}{W_m^{1/3}} + 2.0 \quad \left( \text{Crater and spall } 2.0 \leq \frac{T}{W_m^{1/3}} \leq 3.6 \right) \quad (5)$$

$$\frac{C_d + S_d}{T} = 1.0 \quad \left( \text{Breach } \frac{T}{W_m^{1/3}} \leq 2.0 \right) \quad (6)$$

where  $C_d$  (cm) is depth of the crater and  $S_d$  (cm) is depth of the spall.

Figure 16 compares the experimental results of the failure mode with the empirical equations. From the figure, it can be seen that although the failure modes of the NHC and NCC panels by the experimental results are well agreed with the empirical equations, whereas the blast resistance of FRCC panels are underestimated. Similar observations were previously reported by Li et al. (2016): the failure modes of micro steel-fiber-reinforced ultra-high performance concrete slabs are underestimated compared to normal strength concrete subjected to contact explosions, which are predicted from the empirical equations by Li et al. (2016) analyzed to be due to empirical predictions do not consider the effects of fiber reinforcement, which affect the local damage of concrete slabs. Therefore, the blast resistance of FRCCs calculated from empirical predictions are underestimated compared to that of real performance of FRCCs. Consequentially, in the current study, it is also clear that the experimental results of the total depth of local damage in the FRCC panels were significantly lower than those in the plain panels. This implies that the FRCC panels experience not only reduced crater damage, but also reduced spall damage, which reduces the allowable limit thickness for each failure mode under contact explosions.

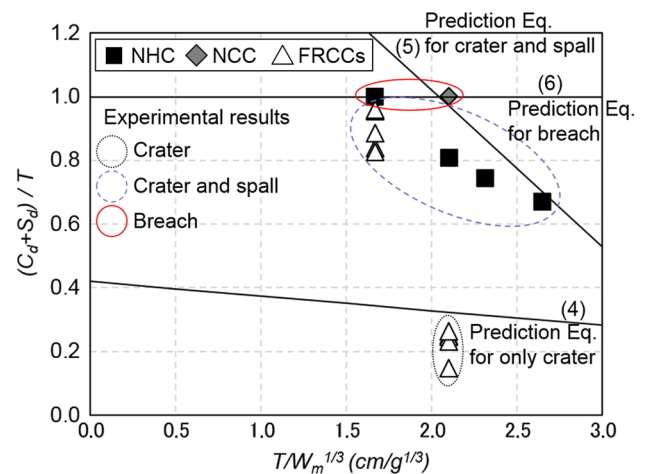


**Fig. 16** Comparison of experimental results with empirical equations for failure mode.

## 4. Conclusions

The objective of this study was to experimentally clarify the effect of fiber reinforcements on the local damage of FRCC panels subjected to contact explosions. Five kinds of FRCCs were investigated in the study. Based on the experimental results, the main findings of this study, which are useful information for blast resistance of FRCCs, are drawn as follows:

1. For FRCCs, the fracture energy of PVASCC and PESCC is greater than that of SCC, which shows the influence of hybrid macro and micro fiber on FRCC flexural performance. Additionally, comparing the flexural performance of FRCCs to that of the plain specimens, the fracture energy of FRCCs is significantly larger than that of NHC and NCC. By having increased fracture energy, FRCCs have superior resistance to local damage under contact explosions, which suppresses the propagation of wide radial cracks to the back sides of the panels.
2. The experimental results revealed that FRCC panels have high resistance to failure under contact explosions as compared with plain panels. Specifically, for contact explosions using 100 g of blast charge, the cracks observed on the SCC panel were more prevalent than for the other FRCC panels, but these cracks were still controlled by hybrid blending with micro synthetic fibers (1 vol.% macro hooked-end steel fibers and 1 vol.% micro synthetic fibers). Therefore, the hybrid blending of fibers plays an important role in the blast resistance of FRCC panels.
3. The fiber reinforcements of FRCC panels significantly reduce the damage diameter and amount of superficial damage as compared to depth of the local damage. This implies that the influence of fiber reinforcement in FRCCs on the blast resistance is associated with the restraint of the lateral progress of local damage. Based on the relationship between crater and spall, the diameter/depth ratios of local damage in FRCC panels were more closely distributed in crater areas in contrast to those of plain panels. Thus, FRCCs should experience a reduced damage area on the back side of panels even if spall or breach occurs.
4. Finally, the experimental results presented useful data for comparison to empirical equations for prediction of limited thickness on the local damage subjected to contact explosions. The experimental results for the total depth of local damage in the FRCC panels were significantly lower than those in the plain panels, which implies that the FRCC panels restrain the critical local damage. However, it should be noted that these empirical methods tend to greatly underestimate the blast resistance of FRCC panels due to do not consider the effects of fiber reinforcements.

## Acknowledgements

This work was supported by the Basic Science Research Program through the National Research Foundation of Korea (NRF) funded by the Ministry of Science, Information

and Communications Technologies (ICT) & Future Planning (No. 2015R1A5A1037548).

## Open Access

This article is distributed under the terms of the Creative Commons Attribution 4.0 International License (<http://creativecommons.org/licenses/by/4.0/>), which permits unrestricted use, distribution, and reproduction in any medium, provided you give appropriate credit to the original author(s) and the source, provide a link to the Creative Commons license, and indicate if changes were made.

## References

- Ahmed, S. F. U., Maalej, M., & Paramasivam, P. (2007). Flexural responses of hybrid steel-polyethylene fiber reinforced cement composites containing high volume fly ash. *Construction and Building Materials*, 21, 1088–1097.
- ASTM C150/C150M. (2016). *Standard specification for Portland cement*. West Conshohocken, PA: ASTM International.
- ASTM C39/C39M. (2015). *Standard test method for compressive strength of cylindrical concrete specimen*. West Conshohocken, PA: ASTM International.
- ASTM C469/C469M. (2014). *Standard test method for static modulus of elasticity and Poisson's ratio of concrete in compression*. West Conshohocken, PA: ASTM International.
- ASTM C618. (2015). *Standard specification for coal fly ash and raw or calcined natural pozzolan for use in concrete*. Conshohocken, PA: ASTM International.
- Atiş, C. D., & Karahan, O. (2009). Properties of steel fiber reinforced fly ash concrete. *Construction and Building Materials*, 23, 392–399.
- Coughlin, A. M., Musselman, E. S., Schokker, A. J., & Linzell, D. G. (2010). Behavior of portable fiber reinforced concrete vehicle barriers subject to blasts from contact charges. *International Journal of Impact Engineering*, 37, 521–529.
- Ha, J. H., Yi, N. H., Choi, J. K., & Kim, J. H. J. (2011). Experimental study on hybrid CFRP-PU strengthening effect on RC panels under blast loading. *Composite Structures*, 93, 2070–2082.
- Habel, K., & Gauvreau, P. (2008). Response of ultra-high performance fiber reinforced concrete (UHPFRC) to impact and static loading. *Cement & Concrete Composites*, 30, 938–946.
- Hanhwa Corporation/Explosive. Explosives Products. Available online: [http://www.hanwhacorp.co.kr/explosives/business/area2\\_1.jsp](http://www.hanwhacorp.co.kr/explosives/business/area2_1.jsp). Accessed on 14 Oct 2016. (In Korean).
- Islam, A. K. M. A., & Yazdani, N. (2008). Performance of AASHTO girder bridges under blast loadings. *Engineering Structures*, 30(7), 1922–1937.
- Kim, H., Kim, G., Gucunski, N., Nam, J., & Jeon, J. (2015a). Assessment of flexural toughness and impact resistance of

- bundle-type polyamide fiber-reinforced concrete. *Composites Part B Engineering*, 78, 431–446.
- Kim, H., Kim, G., Nam, J., Kim, J., Han, S., & Lee, S. (2015b). Static mechanical properties and impact resistance of amorphous metallic fiber-reinforced concrete. *Composite Structures*, 134, 831–844.
- Lan, S., Lok, T. S., & Heng, L. (2005). Composite structural panels subjected to explosive loading. *Construction and Building Materials*, 19, 387–395.
- Lawler, J. S., Wilhelm, T., Zampini, D., & Shah, S. P. (2003). Fracture process of hybrid fiber reinforced mortar. *Materials and Structures*, 36, 197–208.
- Lee, J., & Lopez, M. M. (2014). An experimental study on fracture energy of plain concrete. *International Journal of Concrete Structures and Materials*, 8(2), 129–139.
- Leppänen, J. (2006). Concrete subjected to projectile and fragment impacts: Modelling of crack softening and strain rate dependency in tension. *International Journal of Impact Engineering*, 32, 1828–1841.
- Li, V., & Stang, H. (1997). Interface property characterization and strengthening mechanisms in fiber reinforced cement based composites. *Advanced Cement Based Materials*, 6(1), 1–20.
- Li, J., Wu, C., Hao, H., Su, Y., & Liu, Z. (2016a). Blast resistance of concrete slab reinforced with high performance fibre material. *Journal of Structural Integrity and Maintenance*, 1(2), 51–59.
- Li, J., Wu, C., Hao, H., Wang, Z., & Su, Y. (2016b). Experimental investigation of ultra-high performance concrete slabs under contact explosions. *International Journal of Impact Engineering*, 93, 62–75.
- Luccioni, B. M., Ambrosini, R. D., & Danesi, R. F. (2004). Analysis of building collapse under blast loads. *Engineering Structures*, 26(1), 63–71.
- Mahmoud, E., Ibrahim, A., El-Chabib, H., & Patibandla, V. C. (2013). Self-consolidating concrete incorporating high volume of fly ash, slag, and recycled asphalt pavement. *International Journal of Concrete Structures and Materials*, 7(2), 155–163.
- McVay, M. K. (1988). Spall damage of concrete structures. U.S. Army Corps of Engineers Waterways Experimental Station, Technical report SL88-22.
- Mechtcherine, V., Millon, O., Butler, M., & Thoma, K. (2011). Mechanical behaviour of strain hardening cement-based composites under impact loading. *Cement & Concrete Composites*, 33, 1–11.
- Mindess, S., Banthia, N., & Yan, C. (1987). The fracture toughness of concrete under impact loading. *Cement and Concrete Research*, 17(2), 231–241.
- Morishita, M., Tanaka, H., Ando, T., & Hagiya, H. (2004). Effects of concrete strength and reinforcing clear distance on the damage of reinforced concrete slabs subjected to contact detonations. *Concrete Research and Technology*, 15(2), 89–98. (in Japanese).
- Morishita, M., Tanaka, H., Itoh, T., & Yamaguchi, H. (2000). Damage of reinforced concrete slabs subjected to contact detonations. *Journal of Structural Engineering*, 46A, 1787–1797. (in Japanese).
- Mosalam, K. M., & Mosallam, A. S. (2001). Nonlinear transient analysis of reinforced concrete slabs subjected to blast loading and retrofitted with CFRP composites. *Composites Part B Engineering*, 32, 623–636.
- Naaman, A. E. (2003). Engineered steel fibers with optimal properties for reinforcement of cement composites. *Journal of Advanced Concrete Technology*, 1(3), 241–252.
- Nam, J. W., Kim, H. J., Kim, S. B., Yi, N. H., & Kim, J. H. J. (2010). Numerical evaluation of the retrofit effectiveness for GFRP retrofitted concrete slab subjected to blast pressure. *Composite Structures*, 92, 1212–1222.
- Nam, J. S., Kim, G. Y., Miyauchi, H., Jeon, Y. S., & Hwang, H. K. (2011). Evaluation on the blast resistance of fiber reinforced concrete. *Advanced Materials Research*, 311–313, 1588–1593.
- Nam, J., Shinohara, Y., Atou, T., Kim, H., & Kim, G. (2016). Comparative assessment of failure characteristics on fiber-reinforced cementitious composite panels under high-velocity impact. *Composites Part B Engineering*, 99, 84–97.
- Ohkubo, K., Beppu, M., Ohno, T., & Satoh, K. (2008). Experimental study on the effectiveness of fiber sheet reinforcement on the explosive-resistant performance of concrete plates. *International Journal of Impact Engineering*, 35, 1702–1708.
- Ohtsu, M., Uddin, F. A. K. M., Tong, W., & Murakami, K. (2007). Dynamics of spall failure in fiber reinforced concrete due to blasting. *Construction and Building Materials*, 21, 511–518.
- Osteraas, J. D. (2006). Murrah building bombing revisited: a qualitative assessment of blast damage and collapse patterns. *Journal of Performance of Constructed Facilities*, 20(4), 330–335.
- Razaqpur, A. G., Tolba, A., & Contestabile, E. (2007). Blast loading response of reinforced concrete panels reinforced with externally bonded GFRP laminates. *Composites Part B Engineering*, 38, 535–546.
- RILEM 50-FMC Draft Recommendation. (1985). Determination of the fracture energy of mortar and concrete by means of three-point bend tests on notched beams. *Materials and Structures*, 18(106), 285–290.
- Shu, X., Graham, R. K., Huang, B., & Burdette, E. G. (2015). Hybrid effects of carbon fibers on mechanical properties of Portland cement mortar. *Materials and Design*, 65, 1222–1228.
- Silva, P. F., & Lu, B. (2007). Improving the blast resistance capacity of RC slabs with innovative composite materials. *Composites Part B Engineering*, 38, 523–534.
- Silva, P. F., & Lu, B. (2009). Blast resistance capacity of reinforced concrete slabs. *Journal of Structural Engineering*, 135, 708–716.
- Soe, K. T., Zhang, Y. X., & Zhang, L. C. (2013). Impact resistance of hybrid-fiber engineered cementitious composite panels. *Composite Structures*, 104, 320–330.
- Tanaka, H., & Tuji, M. (2003). Effects of reinforcing on damage of reinforced concrete slabs subjected to explosive loading. *Concrete Research and Technology*, 14(1), 1–11. (in Japanese).

- van Doormaal, J. C. A. M., Weerheijm, J., & Sluys, L. J. (1994). Experimental and numerical determination of the dynamic fracture energy of concrete. *Journal de Physique IV*, 4(C8), 501–506.
- Wang, W., Zhang, D., Lu, F., Wang, S. C., & Tang, F. (2013). Experimental study and numerical simulation of the damage mode of a square reinforced concrete slab under close-in explosion. *Engineering Failure Analysis*, 27, 41–51.
- Wu, C., Nurwidayati, R., & Oehlers, D. J. (2009a). Fragmentation from spallation of RC slabs due to airblast loads. *International Journal of Impact Engineering*, 36, 1371–1376.
- Wu, C., Oehlers, D. J., Rebentrost, M., Leach, J., & Whittaker, A. S. (2009b). Blast testing of ultra-high performance fibre and FRP-retrofitted concrete slabs. *Engineering Structures*, 31, 2060–2069.
- Xie, W., Jiang, M., Chen, H., Zhou, J., Xu, Y., Wang, P., et al. (2014). Experimental behaviors of CFRP cloth strengthened buried arch structure subjected to subsurface localized explosion. *Composite Structures*, 116, 562–570.
- Yamaguchi, M., Murakami, K., Takeda, K., & Mitsui, Y. (2011). Blast resistance of polyethylene fiber reinforced concrete to contact detonation. *Journal of Advanced Concrete Technology*, 9(1), 63–71.
- Yang, E. H., Yang, Y., & Li, V. C. (2007). Use of high volumes of fly ash to improve ECC mechanical properties and material greenness. *ACI Materials Journal*, 104(6), 620–628.
- Yoo, D. Y., Banthia, N., Kim, S. W., & Yoon, Y. S. (2015). Response of ultra-high-performance fiber-reinforced concrete beams with continuous steel reinforcement subjected to low-velocity impact loading. *Composite Structures*, 126, 233–245.
- Yoo, D. Y., & Yoon, Y. S. (2016). A review on structural behavior, design, and application of ultra-high-performance fiber-reinforced concrete. *International Journal of Concrete Structures and Materials*, 10(2), 125–142.
- Zhang, X. X., Ruiz, G., Yu, R. C., & Tarifa, M. (2009). Fracture behaviour of high-strength concrete at a wide range of loading rates. *International Journal of Impact Engineering*, 36, 1204–1209.